A WELL-BALANCED AND ENTROPY STABLE SCHEME FOR A REDUCED BLOOD FLOW MODEL

RAIMUND BÜRGER^A, SONIA VALBUENA^B, AND CARLOS A. VEGA^{C,*}

ABSTRACT. A well-known reduced model of the flow of blood in arteries can be formulated as a strictly hyperbolic system of two scalar balance law in one space dimension where the unknowns are the cross-sectional area of the artery and the average blood flow velocity as functions of the axial coordinate and time. This system is endowed with an entropy pair such that solutions of the balance equations satisfy an entropy inequality in the distributional sense. It is demonstrated that this property can be utilized to construct an entropy stable finite difference scheme for the blood flow model based on the general framework by Tadmor [E. Tadmor, The numerical viscosity of entropy stable schemes for systems of conservation laws, I, Math. Comput., 49 (1987) pp. 91–103]. Furthermore, a fourth-order extension of the resulting entropy conservative flux and a fourth-order sign-preserving reconstruction of the scaled entropy variables are employed as well as a second-order strong stability preserving Runge-Kutta method for time discretization. The result is computationally inexpensive and easy-to-implement explicit entropy stable scheme for the blood low model. It is proven that the scheme is well-balanced (i.e., preserves certain steady solutions of the model) and numerical examples are presented.

1. Introduction

1.1. **Scope.** The flow of blood in axisymmetric vessels with compliant walls and flat velocity profile can be described by the following one-dimensional (1D)reduced model (see [1]):

$$\partial_t A + \partial_x (AU) = 0, \quad \partial_t U + U \partial_x U = \frac{1}{\rho} \partial_x P + \frac{\mathcal{F}}{\rho A}.$$
 (1.1)

Here x is the axial coordinate along the vessel (artery), $A(x,t) = \pi(R(x,t))^2$ is the cross-sectional area where R(x,t) is the local, time-dependent radius of the vessel, U(x,t) is the mean blood velocity in the axial direction, ρ is the blood density, assumed to be constant for blood which is essentially incompressible, P = P(A) is the internal pressure and $\mathcal{F}(x,t)$ is the friction force per unit length. The present work is restricted to the inviscid limit where $\mathcal{F} = 0$ [2]. The system (1.1) is closed by a relationship of the form (see [3]) $P = P_{\text{ext}} + \beta(A^{1/2} - A_0^{1/2})$, where P_{ext} stands for the external pressure (assumed to be constant), the coefficient β , which is supposedly constant as well, accounts for the material properties of the elastic vessel, and $A_0 = A_0(x)$ is the vessel

Date: June 18, 2021.

²⁰¹⁰ Mathematics Subject Classification. 65M06, 76Z05, 92C35.

Keywords. Blood flow model, entropy conservative flux, entropy stable scheme, well-balanced property.

^{*}Corresponding author.

^ACI²MA and Departamento de Ingeniería Matemática, Facultad de Ciencias Físicas y Matemáticas, Universidad de Concepción, Casilla 160-C, Concepción, Chile. E-Mail: rburger@ing-mat.udec.cl.

^BUniversidad del Atlántico, Km.7 Vía Puerto Colombia, Barranquilla, Colombia. E-Mail: soniabalbuena@mail.uniatlantico.edu.co.

^CDepartamento de Matemáticas y Estadística, Universidad del Norte, Km.5 Vía Puerto Colombia, Barranquilla, Colombia. E-Mail: cvega@uninorte.edu.co.

cross-sectional area at rest, which may be variable in the case of aneurism, stenosis or taper. In light of the previous discussion we may rewrite (1.1) in the form

$$\partial_t A + \partial_x (AU) = 0, \quad \partial_t U + \partial_x \left(\frac{U^2}{2} + \frac{\beta}{\rho} A^{1/2}\right) = \frac{\beta}{\rho} \partial_x A_0^{1/2}.$$
 (1.2)

The system (1.2) is known as the (A, U)-system. The velocity U is not a conservative quantity, in contrast to Q = AU within the so-called (A, Q)-system [4]. For continuous solutions, the two formulations are equivalent. We will only discuss the (A, U)-system which has a simpler structure.

The system (1.2) can be written as a system of balance laws

$$\partial_t \boldsymbol{w} + \partial_x \boldsymbol{f}(\boldsymbol{w}) = \boldsymbol{S}(x), \tag{1.3}$$

where

conservation laws

$$\boldsymbol{w} = \begin{pmatrix} A \\ U \end{pmatrix}, \quad \boldsymbol{f}(\boldsymbol{w}) = \begin{pmatrix} AU \\ \frac{U^2}{2} + \frac{\beta}{\rho} A^{1/2} \end{pmatrix}, \quad \text{and} \quad \boldsymbol{S}(x) = \begin{pmatrix} 0 \\ \frac{\beta}{\rho} \partial_x A_0^{1/2} \end{pmatrix}$$

The quasilinear form is $\partial_t \mathbf{w} + \mathbf{H}(\mathbf{w}) \partial_x \mathbf{w} = \mathbf{S}(x)$, where

$$\boldsymbol{H}(\boldsymbol{w}) = \begin{bmatrix} U & A \\ c^2/A & U \end{bmatrix}, \quad c := \left(\frac{\beta A^{1/2}}{2\rho}\right)^{1/2},$$

is the Jacobian of f, where c = c(A) is the well-known Moens-Korteweg wave speed.

For A > 0, which is a necessary condition to have a physically relevant solution, the matrix \mathbf{H} has two real and distinct eigenvalues $\lambda_1 = U - c$ and $\lambda_2 = U + c$. Consequently, the system (1.2) is strictly hyperbolic. The associated right eigenvectors are given by

$$\mathbf{r}_{1}^{\mathrm{T}} = (-1, c/A) \text{ and } \mathbf{r}_{2}^{\mathrm{T}} = (1, c/A).$$
 (1.4)

The system (1.2) admits the following steady-state solution, known as the *(non-zero pressure)* man-at-eternal-rest steady state or dead-man equilibrium [4] (by analogy to the lake at rest in the shallow water equations):

$$U = 0$$
 and $A^{1/2} - A_0^{1/2} = C = \text{constant}.$ (1.5)

In particular, the *(zero pressure) man-at-eternal-rest* steady state is given by (1.5) with C = 0. Let us also recall that a convex scalar function $\eta = \eta(\mathbf{w}) \in C^1$ is an entropy for the system of

$$\partial_t \boldsymbol{w} + \partial_x \boldsymbol{f}(\boldsymbol{w}) = \boldsymbol{0},\tag{1.6}$$

if there exists an associated entropy flux G = G(w) that satisfies

$$\nabla G(\boldsymbol{w}) = \boldsymbol{v}^{\mathrm{T}} \boldsymbol{H}(\boldsymbol{w}), \tag{1.7}$$

where $\mathbf{v} = \nabla \eta(\mathbf{w})$ is the vector of entropy variables. If a function G satisfying (1.7) exists then (η, G) is called an entropy pair for the conservation law (1.6). We will also use the *entropy potential*

$$\psi(\mathbf{w}) := \langle \mathbf{v}, \mathbf{f}(\mathbf{w}) \rangle - G(\mathbf{w}). \tag{1.8}$$

This function plays an important role in the construction of entropy conservative fluxes.

A system of conservation laws (1.6) endowed with an entropy pair satisfies the additional conservation law

$$\partial_t \eta(\mathbf{w}) + \partial_x G(\mathbf{w}) = 0 \tag{1.9}$$

for smooth solutions. However, it is well known that solutions of (1.6) develop discontinuities, therefore the entropy equation (1.9) transforms into the entropy inequality $\partial_t \eta(\mathbf{w}) + \partial_x G(\mathbf{w}) \leq 0$

in the sense of distributions. This entropy condition singles out a unique solution and it is useful to obtain energy inequalities.

For the inviscid (A, U) system (1.2), Formaggia et al. [5] derived the entropy pair

$$\eta = \frac{1}{2}AU^2 + \frac{2\beta A^{3/2}}{3\rho}, \quad G = \frac{1}{2}AU^3 + \frac{\beta UA^{3/2}}{\rho},$$
(1.10)

with the corresponding entropy variables

$$\boldsymbol{v}(\boldsymbol{w}) = \left(\frac{U^2}{2} + \frac{\beta}{\rho} A^{1/2}, AU\right)^{\mathrm{T}}$$
(1.11)

and the entropy potential

$$\psi(\mathbf{w}) = \frac{AU^3}{2} + \frac{\beta U A^{3/2}}{\rho}.$$
 (1.12)

The entropy pair (1.10) can be extended to a new entropy pair $(\hat{\eta}, \hat{G})$ (see [6]) to take into account the term S(x):

$$\hat{\eta} = \frac{1}{2}AU^2 + \frac{2\beta A^{3/2}}{3\rho} - \frac{\beta A_0^{1/2}}{\rho}A, \qquad \hat{G} = \frac{1}{2}AU^3 + \frac{\beta U A^{3/2}}{\rho} - \frac{\beta A_0^{1/2}}{\rho}AU.$$
 (1.13)

Thus, the discontinuous solution w of the balanced law (1.3) satisfies the distributional entropy inequality

$$\partial_t \hat{\eta}(x, \boldsymbol{w}) + \partial_x \hat{G}(x, \boldsymbol{w}) \le 0.$$
 (1.14)

It is the purpose of this contribution to advance a numerical scheme for (1.1), supplied with suitable initial conditions, that in semi-discrete (i.e., discrete in space but continuous in time) form satisfies an analogue of (1.14). Such entropy conservative (EC) schemes were introduced by Tadmor [7] for systems of conservation laws and play an essential role in the construction of entropy stable (ES) schemes, since a scheme that contains more numerical viscosity than an entropy conservative scheme is entropy stable [7, Th. 5.2]. Furthermore, a fourth-order extension of the resulting entropy conservative flux and a fourth-order sign-preserving reconstruction of the scaled entropy variables are employed as well as a second-order strong stability preserving Runge-Kutta method for time discretization. The result is computationally inexpensive and easy-to-implement explicit entropy stable scheme and well-balanced scheme for the blood flow model.

1.2. Related work. To put the present contribution into the proper perpective, we mention that numerical solutions of 1D blood flow models have gained considerable importance in recent years because they can be coupled with 3D models to obtain a considerable reduction of the computational complexity [5]. Furthermore, algebraic relationships between P and A alternative to our choice can be found in [8, 9]. Contributions to the numerical solution of the (A, U)-system can be found in [1,4,10] using discontinuous Galerkin, Taylor-Galerkin and some kind of well-balanced property finite volume schemes. An unconditionally stable method based on characteristics variables was developed in [11]. In [12] a complete numerical comparison of six numerical schemes applied to the (A, U)-system is developed. More recently, Wang et al. [13] advanced well-balanced finite difference weighted essentially non-oscillatory (WENO) schemes for the blood flow model in the (A, Q) formulation, and Puelz et al. [14] presented a systematic comparison between (A, U) and (A, Q) systems using Runge-Kutta discontinuous Galerkin methods.

With respect expositions of entropy stable schemes for conservation laws we refer, besides the original works by Tadmor [7,15], to later developments including the combination with high-order diffusion operators [16], the construction of high-order entropy conservative fluxes [17], extensions

to non-conservative hyperbolic systems [18,19], discontinuous Galerkin schemes [20], and shallow water models [21,22]. We also refer to the handbook entry [23] and recent textbook chapter [24, Sect. 8.2.2]. Certain multi-species kinematic flow models (e.g., of vehicular traffic [25,26]) lead to first-order systems of conservation laws of arbitrary size that are endowed with an entropy pair and admit the construction of entropy stable schemes [27]. Such schemes can even be applied to certain systems of degenerate parabolic equations [28], although the class of diffusion coefficients compatible with the entropy variable framework is very narrow, as is elaborated in [29].

1.3. Outline of the paper. The remainder of this paper is organized as follows. Section 2 contains a brief summary of theory about entropy conservative schemes developed by Tadmor [7,15]. Then we utilize this general framework to construct an entropy conservative scheme for the inviscid (A, U)-system. Section 3 will be devoted to prove that the proposed scheme is well-balanced and entropy conservative. To this end, we employ similar arguments to those set out in [21] to the case of shallow water equations. In Section 4 we follow the general procedure that is proposed in [16] to ensure entropy stability of the proposed scheme. Numerical experiments demonstrating the performance of the well-balanced and entropy stable scheme are presented in Section 5. Finally, some conclusions are drawn in Section 6.

2. Entropy conservative numerical schemes

A semi-discrete finite volume scheme for (1.6) on a uniform spatial mesh with nodes $x_j = j\Delta x$, $j \in \mathbb{Z}$ is given by

$$\frac{\mathrm{d}\boldsymbol{w}_{j}(t)}{\mathrm{d}t} = -\frac{1}{\Delta x} \left(\boldsymbol{F}_{j+1/2} - \boldsymbol{F}_{j-1/2} \right), \quad j \in \mathbb{Z}, \tag{2.1}$$

where $w_j(t)$ is the cell average on $I_j = [x_{j-1/2}, x_{j+1/2}]$ and $F_{j+1/2} = F(w_{j-p+1}, \dots, w_{j+p})$ is the numerical flux associated with $x_{j+1/2}$. We assume that $F_{j+1/2}$ is a Lipschitz continuous function and consistent with the differential flux in the standard sense, *i.e.* $F(w, w, \dots, w) = f(w)$.

The scheme (2.1) is called *entropy stable* with respect to the entropy pair (η, G) if it satisfies a discrete entropy inequality

$$\frac{\mathrm{d}}{\mathrm{d}t}\eta(\boldsymbol{w}_{j}(t)) + \frac{1}{\Delta x} \left(\tilde{G}_{j+1/2} - \tilde{G}_{j-1/2} \right) \le 0$$
(2.2)

for some numerical entropy flux $\tilde{G}_{j+1/2}$ consistent with the entropy flux G. If equality holds in (2.2), then the scheme (2.1) is called entropy conservative.

Let us recall a basic result to design entropy preserving numerical fluxes. In the sequel, we use the following the notation

$$[\![a]\!]_{j+1/2} := a_{j+1} - a_j, \qquad \overline{a}_{j+1/2} := \frac{1}{2}(a_{j+1} + a_j),$$

where $[a]_{j+1/2}$ represents the jump of a across the interface at $x_{j+1/2}$

Theorem 1 (cf. Tadmor [7]). Assume that the one-dimensional system of conservation laws (1.6) is endowed with an entropy pair (η, G) . Suppose that $\tilde{\mathbf{F}}_{j+1/2}$ is a consistent numerical flux that satisfies

$$\left\langle \llbracket \boldsymbol{v} \rrbracket_{j+1/2}, \tilde{\boldsymbol{F}}_{j+1/2} \right\rangle = \llbracket \psi \rrbracket_{j+1/2}, \quad j \in \mathbb{Z}. \tag{2.3}$$

where ψ is defined by (1.8). Then the numerical scheme

$$\frac{\mathrm{d}\boldsymbol{w}_{j}(t)}{\mathrm{d}t} = -\frac{1}{\Delta x} (\tilde{\boldsymbol{F}}_{j+1/2} - \tilde{\boldsymbol{F}}_{j-1/2}), \quad j \in \mathbb{Z},$$

is second-order accurate and entropy conservative, and satisfies the discrete entropy identity

$$\frac{\mathrm{d}}{\mathrm{d}t}\eta(\boldsymbol{w}_j(t)) = -\frac{1}{\Delta x} (\tilde{G}_{j+1/2} - \tilde{G}_{j-1/2}), \quad j \in \mathbb{Z},$$

with the numerical entropy flux

$$\tilde{G}_{j+1/2} = \langle \bar{\boldsymbol{v}}_{j+1/2}, \tilde{\boldsymbol{F}}_{j+1/2} \rangle - \bar{\psi}_{j+1/2}.$$
 (2.4)

To construct an entropy conservative flux at the interface $x_{j+1/2}$ for the (A, U)-system the strategy proposed in [22] for the shallow water equations will be used. This strategy is called Explicit Energy Conservative (EEC) flux. Using the following identity between jumps and averages,

$$[\![ab]\!]_{j+1/2} = \bar{b}_{j+1/2} [\![a]\!]_{j+1/2} + [\![b]\!]_{j+1/2} \bar{a}_{j+1/2},$$

we may express the jump of the entropy potential (1.12) across $x_{j+1/2}$ as

On the other hand, the vector-valued jump of entropy variables (1.11) can be written as

$$[\![\boldsymbol{v}]\!]_{j+1/2} = \left(\overline{U}_{j+1/2}[\![\boldsymbol{U}]\!]_{j+1/2} + \frac{\beta}{\rho}[\![\boldsymbol{A}^{1/2}]\!]_{j+1/2}, [\![\boldsymbol{A}\boldsymbol{U}]\!]_{j+1/2}\right)^{\mathrm{T}}.$$

Writing the desired flux componentwise as

$$\tilde{\boldsymbol{F}}_{j+1/2} = (\tilde{F}_{1,j+1/2}, \tilde{F}_{2,j+1/2})^{\mathrm{T}}$$

(in this case), inserting the above two quantities $\llbracket \psi \rrbracket_{j+1/2}$ and $\llbracket \boldsymbol{v} \rrbracket_{j+1/2}$ into (2.3) and then solving the resulting system, we get

$$\tilde{F}_{1,j+1/2} = \overline{(AU)}_{j+1/2}, \quad \tilde{F}_{2,j+1/2} = \frac{1}{2} \overline{(U^2)}_{j+1/2} + \frac{\beta}{\rho} \overline{(A^{1/2})}_{j+1/2}.$$
 (2.5)

This flux is clearly consistent, very simple to code, and computationally inexpensive. However, the two-point entropy conservative fluxes obtained from (2.3) are only second-order accurate. As an improvement of this limitation, LeFloch et al. [17] proposed a procedure to construct 2p-th order entropy conservative fluxes by linear combinations of two-point entropy conservative fluxes $\tilde{\mathbf{F}}$. For instance, the fourth-order entropy conservative flux corresponding to p=2 is given by

$$\tilde{\mathbf{F}}_{j+1/2}^{4} = \frac{4}{3}\tilde{\mathbf{F}}(\mathbf{w}_{j}, \mathbf{w}_{j+1}) - \frac{1}{6}(\tilde{\mathbf{F}}(\mathbf{w}_{j-1}, \mathbf{w}_{j+1}) + \tilde{\mathbf{F}}(\mathbf{w}_{j}, \mathbf{w}_{j+2})). \tag{2.6}$$

3. A Well-balanced entropy conservative scheme

The source term S(x) is discretized by the standard centered difference approximation

$$S_{j} = \frac{\beta}{\rho} \frac{1}{12\Delta x} \begin{pmatrix} 0 \\ A_{0,j-2}^{1/2} - 8A_{0,j-1}^{1/2} + 8A_{0,j+1}^{1/2} - A_{0,j+2}^{1/2} \end{pmatrix}, \tag{3.1}$$

which is fourth-order accurate for smooth solutions. Here $A_{0,j} = A_0(x_j)$. Then the finite volume entropy conservative scheme for (1.3) in its semi-discrete form is

$$\frac{\mathrm{d}\boldsymbol{w}_{j}(t)}{\mathrm{d}t} = -\frac{1}{\Delta x} (\tilde{\boldsymbol{F}}_{j+1/2}^{4} - \tilde{\boldsymbol{F}}_{j-1/2}^{4}) + \boldsymbol{S}_{j}, \tag{3.2}$$

where $\tilde{\boldsymbol{F}}_{j+1/2}^4$ is given by (2.6) and (2.5). The next result shows that the scheme (3.2) is entropy conservative and well-balanced. The proof is similar in spirit to that of Lemma 2.1 in [21].

Lemma 1. The scheme (3.2) satisfies the following properties:

(i) It is entropy conservative, i.e., satisfies the semi-discrete entropy equality

$$\frac{d\hat{\eta}}{dt} + \frac{1}{\Delta x} (\tilde{H}_{j+1/2} - \tilde{H}_{j-1/2}) = 0, \tag{3.3}$$

where $\hat{\eta}$ is the extended entropy function given by (1.13) and the corresponding numerical entropy flux $\tilde{H}_{i+1/2}$ is given by

$$\tilde{H}_{j+1/2} = \tilde{G}_{j+1/2}^4 + \frac{\beta}{12\rho} \left(A_{0,j}^{1/2} A_{j+2} U_{j+2} - A_{0,j}^{1/2} A_{j+1} U_{j+1} - A_{0,j+1}^{1/2} A_j U_j + A_{0,j+1}^{1/2} A_{j-1} U_{j-1} + A_{0,j-1}^{1/2} A_{j+1} U_{j+1} - A_{0,j+2}^{1/2} A_j U_j \right),$$

where for $\tilde{G}_{j+1/2}$ as given by (2.4), we define

$$\tilde{G}_{j+1/2}^4 = \frac{4}{3}\tilde{G}(\boldsymbol{w}_j, \boldsymbol{w}_{j+1}) - \frac{1}{6}(\tilde{G}(\boldsymbol{w}_{j-1}, \boldsymbol{w}_{j+1}) + \tilde{G}(\boldsymbol{w}_j, \boldsymbol{w}_{j+2})).$$

(ii) It is well-balanced, that is, it preserves the discrete version of the man-at-eternal-rest (1.5), this means that given the initial data

$$U_j = 0 \quad \text{for all } j, \tag{3.4a}$$

$$A_i^{1/2} - A_{0,i}^{1/2} = C$$
 for all j (3.4b)

with a constant C, then the solution computed by the scheme satisfies $d\mathbf{w}_j/dt = 0$ for all j.

Proof. To prove the first part, we take the inner product of (3.2) with

$$\hat{\boldsymbol{v}}_j = \nabla \hat{\eta}(\boldsymbol{w}_j) = \boldsymbol{v}_j - \left(\beta A_{0,j}^{1/2}/\rho, 0\right)^{\mathrm{T}},$$

which yields

$$\frac{\mathrm{d}\hat{\eta}(\boldsymbol{w}_{j})}{\mathrm{d}t} = -\frac{1}{\Delta x} \left(\left\langle \boldsymbol{v}_{j}, \tilde{\boldsymbol{F}}_{j+1/2}^{4} - \tilde{\boldsymbol{F}}_{j-1/2}^{4} \right\rangle - \left\langle \left(\beta A_{0,j}^{1/2}/\rho, 0 \right)^{\mathrm{T}}, \tilde{\boldsymbol{F}}_{j+1/2}^{4} - \tilde{\boldsymbol{F}}_{j-1/2}^{4} \right\rangle \right) + \left\langle \hat{\boldsymbol{v}}_{j}, \boldsymbol{S}_{j} \right\rangle.$$

Then, (3.3) is obtained directly from the following equalities:

$$\langle \boldsymbol{v}_{j}, \tilde{\boldsymbol{F}}_{j+1/2}^{4} - \tilde{\boldsymbol{F}}_{j-1/2}^{4} \rangle = \tilde{G}_{j+1/2}^{4} - \tilde{G}_{j-1/2}^{4},$$

$$\langle \left(\beta A_{0,j}^{1/2}/\rho, 0\right)^{\mathrm{T}}, \tilde{\boldsymbol{F}}_{j+1/2}^{4} - \tilde{\boldsymbol{F}}_{j-1/2}^{4} \rangle$$

$$= \frac{\beta}{12\rho} \left(-A_{0,j}^{1/2} A_{j+2} U_{j+2} + 8A_{0,j}^{1/2} A_{j+1} U_{j+1} - 8A_{0,j}^{1/2} A_{j-1} U_{j-1} + A_{0,j}^{1/2} A_{j-2} U_{j-2} \right),$$
and
$$\langle \hat{\boldsymbol{v}}_{j}, \boldsymbol{S}_{j} \rangle = \frac{\beta}{12\rho} \left(A_{0,j-2}^{1/2} A_{j} U_{j} - 8A_{0,j-1}^{1/2} A_{j} U_{j} + 8A_{0,j+1}^{1/2} A_{j} U_{j} - A_{0,j+2}^{1/2} A_{j} U_{j} \right).$$

To prove (ii), assume that the man-at-eternal-rest condition (3.4) is satisfied. Then

$$\tilde{\boldsymbol{F}}_{j+1/2}^4 - \tilde{\boldsymbol{F}}_{j-1/2}^4 = \frac{\beta}{12\rho} \begin{pmatrix} 0 \\ A_{j-2}^{1/2} - 8A_{j-1}^{1/2} + 8A_{j+1}^{1/2} - A_{j+2}^{1/2} \end{pmatrix}$$

Using this expression in (3.2), we get

$$\frac{\mathrm{d}\boldsymbol{w}_{j}(t)}{\mathrm{d}t} = -\frac{\beta}{12\rho\Delta x} \left((A_{j-2}^{1/2} - A_{0,j-2}^{1/2}) - 8(A_{j-1}^{1/2} - A_{0,j-1}^{1/2}) + 8(A_{j+1}^{1/2} - A_{0,j+1}^{1/2}) - (A_{j+2}^{1/2} - A_{0,j+2}^{1/2}) \right) \\
= \begin{pmatrix} 0 \\ 0 \end{pmatrix}.$$

The last equality is a consequence of (3.4b).

4. Entropy stable scheme with high-order diffusion

The entropy conservative schemes discussed in Section 2 perform well approximating smooth solutions, but they lead to high-frequency oscillations in the vicinity of shocks. Therefore, it is necessary to add numerical diffusion to guarantee that entropy is dissipated. To this end, we follow the general procedure proposed by Fjordholm et al. [16] and define the numerical flux i as

$$F_{j+1/2} = \tilde{F}_{j+1/2} - \frac{1}{2} D_{j+1/2} \langle \langle v \rangle \rangle_{j+1/2},$$
 (4.1)

where $\tilde{F}_{j+1/2}$ is an entropy conservative flux, $\langle v \rangle_{j+1/2} := v_{j+1}(x_{j+1/2}) - v_j(x_{j+1/2})$ is the difference in the reconstructed states for some reconstructed function $v_j(x)$ that will be specified later, and $D_{j+1/2}$ is a diffusion matrix of the form

$$D_{j+1/2} = R_{j+1/2} \Lambda_{j+1/2} R_{j+1/2}^{\mathrm{T}}.$$
(4.2)

Here, \mathbf{R} is the matrix of right eigenvectors of the flux Jacobian $\mathbf{H}(\mathbf{w})$ and $\mathbf{\Lambda}$ is the Roe-type diagonal matrix $\mathbf{\Lambda} = \operatorname{diag}(|\lambda_1|, |\lambda_2|)$, where λ_1 and λ_2 are the eigenvalues of the flux Jacobian matrix \mathbf{H} that is evaluated at the average state $\mathbf{w}_{j+1/2} := (\mathbf{w}_j + \mathbf{w}_{j+1})/2$. The following result, which is a special case of a more general theorem due to Barth [31, Theorem 4] (see also [22, Lemma 4.3] for an analogous result applied to the shallow water equations), motivates us to choose the diffusion operator (4.2) as

$$D_{j+1/2} = \tilde{R}_{j+1/2} \Lambda_{j+1/2} \tilde{R}_{j+1/2}^{\mathrm{T}}, \tag{4.3}$$

where $\tilde{\boldsymbol{R}}$ is a matrix of scaled right eigenvectors of \boldsymbol{H} such that $\tilde{\boldsymbol{R}}\tilde{\boldsymbol{R}}^{\mathrm{T}} = \boldsymbol{w}_{\boldsymbol{v}}$, and the notation in (4.3) indicates that all matrices are evaluated at $\boldsymbol{w}_{j+1/2}$.

Lemma 2. Consider the model (1.3) along with the entropy function $\eta(\mathbf{w})$ and entropy variables \mathbf{v} given by (1.10) and (1.11), respectively. Let $\tilde{\mathbf{R}} = [\tilde{\mathbf{r}}_1 \, \tilde{\mathbf{r}}_2]$ be the matrix of the following scaled right eigenvectors of \mathbf{H} :

$$ilde{m{r}}_1 = \left(rac{A}{2c(c-U)}
ight)^{1/2} m{r}_1 \quad and \quad ilde{m{r}}_2 = \left(rac{A}{2c(c+U)}
ight)^{1/2} m{r}_2,$$

where r_1 and r_2 are given by (1.4). Then $\tilde{\boldsymbol{R}}\tilde{\boldsymbol{R}}^{\mathrm{T}} = \boldsymbol{w_v}$, where

$$\boldsymbol{w_v} = \frac{1}{c^2 - U^2} \begin{bmatrix} A & -U \\ -U & c^2/A \end{bmatrix}$$

is the symmetric positive definite change-of-variables matrix.

Proof. The result can be obtained directly by insertion.

Accordingly, we take $\tilde{\mathbf{R}}_{j+1/2}$ as the matrix of scaled right eigenvectors of $\mathbf{H}(\mathbf{w}_{j+1/2})$. For simplicity of notation, we will drop the tilde notation and we use the same letter \mathbf{R} for denoting the matrix of scaled eigenvectors.

In order to maintain entropy stability of the scheme with numerical flux (4.1), entropy variables are reconstructed by using the *scaled entropy variables*

$$oldsymbol{z}_j^\pm := oldsymbol{R}_{j\pm 1/2}^{\mathrm{T}} oldsymbol{v}_j, \qquad oldsymbol{ ilde{z}}_j^\pm := oldsymbol{R}_{j\pm 1/2}^{\mathrm{T}} oldsymbol{v}_j^\pm.$$

Given the interface values of each component $z = z^l$, l = 1, 2, of the scaled entropy variables z for a fixed grid cell I_i , we define the point value $\mu_i^j := z_i^-$, and inductively

$$\mu_{s+1}^j := \mu_s^j + \delta_{s+1/2}, \quad s = j, j+1, \dots; \quad \mu_{s-1}^j := \mu_s^j - \delta_{s+1/2}, \quad s = j, j-1, \dots,$$

where $\delta_{s+1/2} = \langle \langle z \rangle \rangle_{s+1/2}$. Similarly, we define $\nu_j^j := z_j^+$ and

$$\nu_{s+1}^j := \nu_s^j + \delta_{s+1/2}, \quad s = j, j+1, \dots; \quad \nu_{s-1}^j := \nu_s^j - \delta_{s+1/2}, \quad s = j, j-1, \dots$$

Let $\Upsilon_s^j(x) := \mathcal{R}_s(\{\mu_k^j\}_{k \in \mathbb{Z}})$ and $\Psi_s^j(x) := \mathcal{R}_s(\{\nu_k^j\}_{k \in \mathbb{Z}})$ be the reconstructions of μ^j and ν^j in cell I_s . Then the left and right reconstructed values are

$$\tilde{z}_{j}^{-} := \Upsilon_{j}^{j}(x_{j-1/2}) \quad \text{and} \quad \tilde{z}_{j}^{+} := \Psi_{j}^{j}(x_{j+1/2})$$

Since $v_j^{\pm} = (\boldsymbol{R}_{j\pm 1/2}^{\mathrm{T}})^{-1} \tilde{\boldsymbol{z}}_j^{\pm}$, the diffusion term $\boldsymbol{D}_{j+1/2} \langle\!\langle \boldsymbol{v} \rangle\!\rangle_{j+1/2}$ can be expressed as

$$D_{j+1/2} \langle \langle \boldsymbol{v} \rangle \rangle_{j+1/2} = \boldsymbol{R}_{j+1/2} \boldsymbol{\Lambda}_{j+1/2} \boldsymbol{R}_{j+1/2}^{\mathrm{T}} (\boldsymbol{R}_{j+1/2}^{\mathrm{T}})^{-1} \langle \langle \boldsymbol{\tilde{z}} \rangle \rangle_{j+1/2}$$

$$= \boldsymbol{R}_{j+1/2} \boldsymbol{\Lambda}_{j+1/2} \langle \langle \boldsymbol{\tilde{z}} \rangle \rangle_{j+1/2}. \tag{4.4}$$

Then, it is not necessary to compute $(\mathbf{R}_{j\pm1/2}^{\mathrm{T}})^{-1}$ to recover the entropy variables from the scaled entropy variables. As reconstruction procedure, we will use the fourth-order ENO.

Now, the diffusion term $\frac{1}{2}D_{j+1/2}\langle\langle v\rangle\rangle_{j+1/2}$ in (4.1), specified by (4.4), is modified by replacing the entropy variables v given by (1.11) by

$$\hat{\boldsymbol{v}} = \left(\frac{U^2}{2} + \frac{\beta}{\rho} A^{1/2} - \frac{\beta}{\rho} A_0^{1/2}, AU\right)^{\mathrm{T}}.$$

To shorten notation, we continue to write F for the flux obtained in this way. The resulting entropy stable scheme reads

$$\frac{\mathrm{d}\boldsymbol{w}_{j}(t)}{\mathrm{d}t} = -\frac{1}{\Delta x} \left(\boldsymbol{F}_{j+1/2} - \boldsymbol{F}_{j-1/2} \right) + \frac{\beta}{12\rho\Delta x} \begin{pmatrix} 0 \\ A_{0,j-2}^{1/2} - 8A_{0,j-1}^{1/2} + 8A_{0,j+1}^{1/2} - A_{0,j+2}^{1/2} \end{pmatrix}, \quad (4.5)$$

where

$$\mathbf{F}_{j+1/2} = \tilde{\mathbf{F}}^4 - \frac{1}{2} \mathbf{D}_{j+1/2} \langle \langle \hat{\mathbf{v}} \rangle \rangle_{j+1/2}.$$
 (4.6)

This entropy stable scheme, based on a combination of fourth-order entropy conservative flux and fourth-order dissipation operators obtained by using a sign-preserving reconstruction of the scaled entropy variables, is termed as TeCNO4 scheme (see [16]).

Observe that when the data satisfies (3.4), we have $\langle \langle \hat{\boldsymbol{v}} \rangle \rangle_{j+1/2} = 0$ for all j. Thus, the diffusion term in (4.6) vanishes, and we follow the same argument as in the proof of Theorem 1 (ii) to conclude that $d\boldsymbol{w}_j/dt = 0$ for all j. Therefore, the discrete man-at-eternal rest state is preserved.

For second-order accurate integration in time, the explicit second-order strong stability preserving Runge-Kutta method SSPRK will be used [32]. This method is given by the steps

$$w^{(1)} = w^n + \Delta t \mathcal{L}(w^n), \quad w^{(2)} = w^{(1)} + \Delta t \mathcal{L}(w^{(1)}), \quad w^{n+1} = \frac{1}{2}(w^n + w^{(2)}),$$

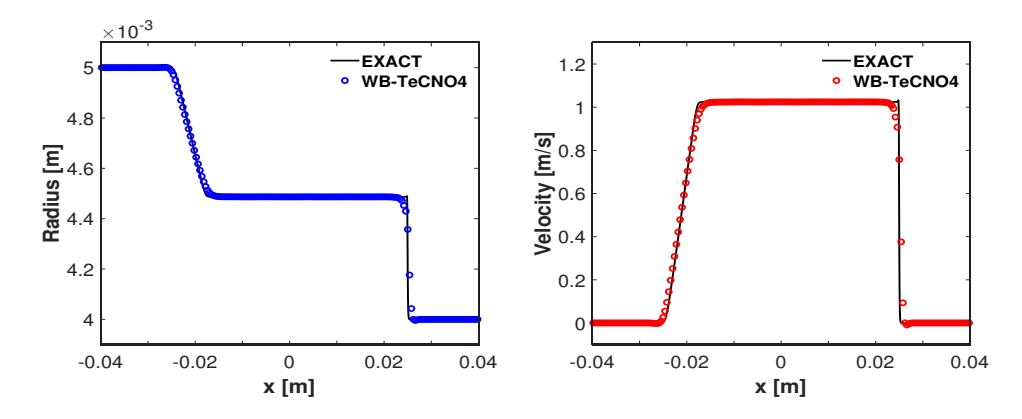


FIGURE 1. Example 1 (ideal tourniquet): numerical solutions of the radius (left) and velocity (right) of the ideal tourniquet problem in Example 5.1 on a mesh with 200 cells at simulated time $t = 0.005 \,\mathrm{s}$.

where

$$[\mathcal{L}(\boldsymbol{w})]_j := -rac{1}{\Delta x} (\hat{\boldsymbol{F}}_{j+1/2} - \hat{\boldsymbol{F}}_{j-1/2}).$$

In all simulations, the CFL number is taken as 0.5.

5. Numerical experiments

We choose several numerical test problems mainly from References [4, 33]. The purpose is to exhibit the performance of the proposed scheme, in particular for testing the well-balanced property. In all numerical experiments, transmissive boundary conditions are imposed. For a deeper discussion of boundary conditions for the blow flow model under study we refer to [10]. The blood density is taken as $\rho = 1060 \,\mathrm{kg/m^3}$.

5.1. Example 1: the ideal tourniquet. This example is an analogue of the dam break problem in shallow water equations. A tourniquet is applied and we remove it immediately. When tourniquet is removed, the blood flows from upstream to downstream in the vessel. The initial conditions are

$$A(x,0) = \begin{cases} \pi R_{\rm L}^2 & \text{for } x \le 0, \\ \pi R_{\rm R}^2 & \text{for } x > 0 \end{cases}$$
 and $U(x,0) = 0.$

 $A(x,0) = \begin{cases} \pi R_{\rm L}^2 & \text{for } x \le 0, \\ \pi R_{\rm R}^2 & \text{for } x > 0 \end{cases} \quad \text{and} \quad U(x,0) = 0,$ with $R_{\rm L} = 5 \times 10^{-3} \, \text{m}$ and $R_{\rm R} = 4 \times 10^{-3} \, \text{m}$. The computational domain is [-0.04, 0.04] (in meters), we choose $\beta = \pi^{-1} \times 10^7 \,\mathrm{Pa/m}$, and the radius at rest of the artery is taken as constant. The solution profiles consist in a left-moving rarefaction wave and right-moving shock wave, as shown in Figure 1. Numerical solutions are computed on a mesh with 200 cells at simulated time $t = 0.005 \,\mathrm{s}$. It can be observed that the results of our well-balanced and entropy stable scheme (denoted by WB-TeCNO4) fit well with the exact ones and keep steep discontinuity transitions at the same time.

Since the solution in this example develops discontinuities, we verify that the method is indeed entropy stable by displaying in Figure 2 the relative change in total entropy for $t = t_n = n\Delta t$

$$\frac{\mathcal{E}(t_n) - \mathcal{E}(0)}{\mathcal{E}(0)}, \quad \text{where} \quad \mathcal{E}(t_n) := \Delta x \sum_{j=1}^{M} \eta(\boldsymbol{w}_j(t_n)). \tag{5.1}$$

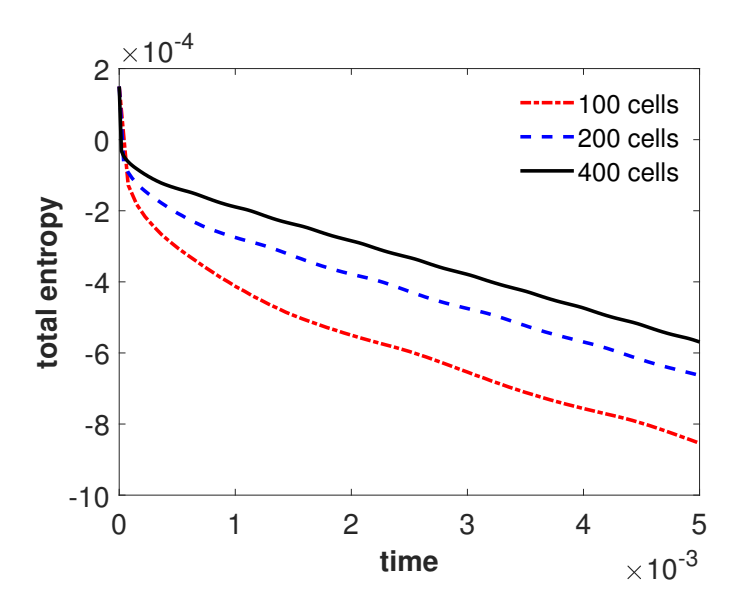


FIGURE 2. Example 1 (ideal tourniquet): relative change in total entropy of numerical solutions on three different mesh sizes.

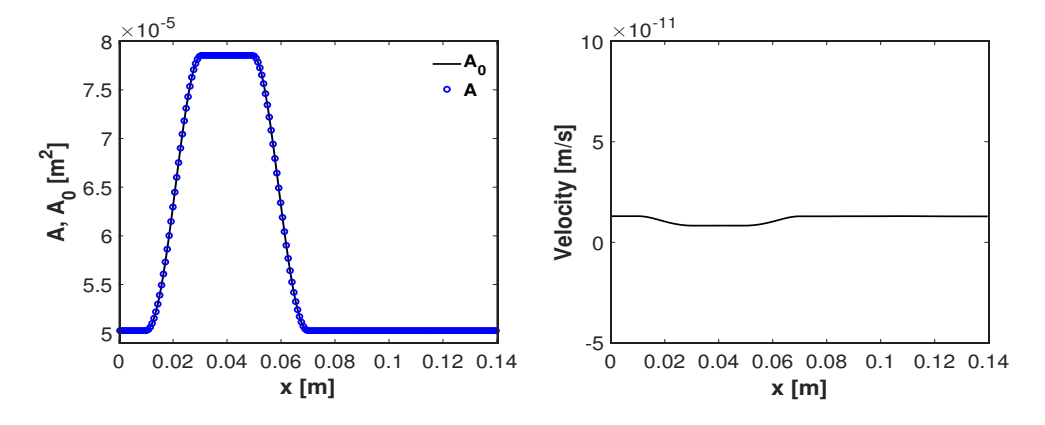


FIGURE 3. Example 2 (zero-pressure steady state): numerical solutions of the zero pressure man-at-eternal-rest problem on a mesh with 200 cells at simulated time t = 5 s. Area and area at rest (left) and velocity (right).

5.2. Example 2: a zero-pressure man-at-eternal-rest steady state. The purpose of this test problem is to check that the proposed scheme preserves the zero pressure man-at-eternal-rest steady state (1.5) with C = 0. The configuration exhibits with no flow and includes a change in the section of the artery. This is the case for a dead man with an aneurism. The initial conditions

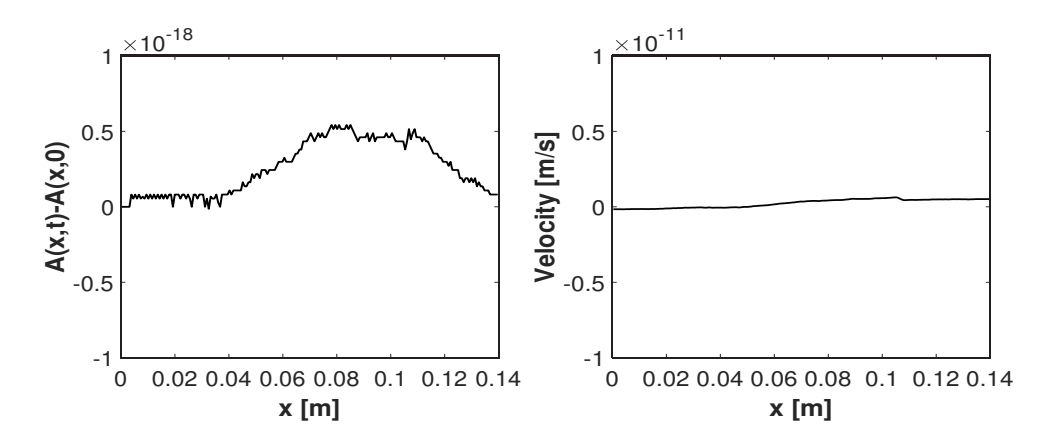


FIGURE 4. Example 3 (non-zero-pressure steady state): numerical solutions of the non-zero pressure man-at-eternal-rest problem on a mesh with 200 cells at simulated time t = 1 s. Area minus area at rest (left) and velocity (right).

are U(x,0)=0 and $A(x,0)=A_0(x)=\pi R_0^2(x),$ where

$$R_0(x) = \begin{cases} \tilde{R} & \text{for } x \in [0, x_1] \cup [x_4, L], \\ \tilde{R} + \frac{\Delta R}{2} \left(\sin \left(\frac{x - x_1}{x_2 - x_1} \pi - \frac{\pi}{2} \right) + 1 \right) & \text{for } x \in (x_1, x_2), \\ \tilde{R} + \Delta R & \text{for } x \in [x_2, x_3], \\ \tilde{R} + \frac{\Delta R}{2} \left(\cos \left(\frac{x - x_3}{x_4 - x_3} \pi \right) + 1 \right) & \text{for } x \in (x_3, x_4) \end{cases}$$

with $\tilde{R}=4\times10^{-3}$ m, $\Delta R=1.0\times10^{-3}$ m, $x_1=1.0\times10^{-2}$ m, $x_2=3.05\times10^{-2}$ m, $x_3=4.95\times10^{-2}$ m, $x_4=7.0\times10^{-2}$ m and L=0.14 m. The computational domain is [0,L] and $\beta=\pi^{-1}\times10^{8}$ Pa/m. Figure 3 shows the area of the artery and the velocity on a mesh with 200 cells at simulated time t=5 s.

5.3. Example 3: a non-zero-pressure man-at-eternal-rest steady state. This example (see [33]) corresponds to the case of a dead man with stenosis. The cross-sectional area at rest is $A_0(x) = \pi R_0^2(x)$, where

$$R_{0}(x) = \begin{cases} \tilde{R} + \Delta R & \text{for } x \in [0, x_{1}] \cup [x_{4}, L], \\ \tilde{R} - \frac{\Delta R}{2} \left(\sin \left(\frac{x - x_{1}}{x_{2} - x_{1}} \pi - \frac{\pi}{2} \right) - 1 \right) & \text{for } x \in (x_{1}, x_{2}), \\ \tilde{R} & \text{for } x \in [x_{2}, x_{3}], \\ \tilde{R} - \frac{\Delta R}{2} \left(\cos \left(\frac{x - x_{3}}{x_{4} - x_{3}} \pi \right) - 1 \right) & \text{for } x \in (x_{3}, x_{4}) \end{cases}$$

with $\tilde{R}=4\times 10^{-3}\,\mathrm{m}$, $\Delta R=1.0\times 10^{-3}\,\mathrm{m}$, an artery of length $L=0.14\,\mathrm{m}$, $x_1=9L/40$, $x_2=L/4$, $x_3=3L/40$, $x_4=31L/40$. The initial conditions are

$$A(x,0) = (C + \pi^{1/2}R_0(x))^2, \qquad U(x,0) = 0,$$

where $C = 10^{-3}$ m. The solution is computed at t = 1 s with a mesh of 200 cells. It can be observed in Figure 4 that the proposed scheme is capable of preserving the non-constant area A.

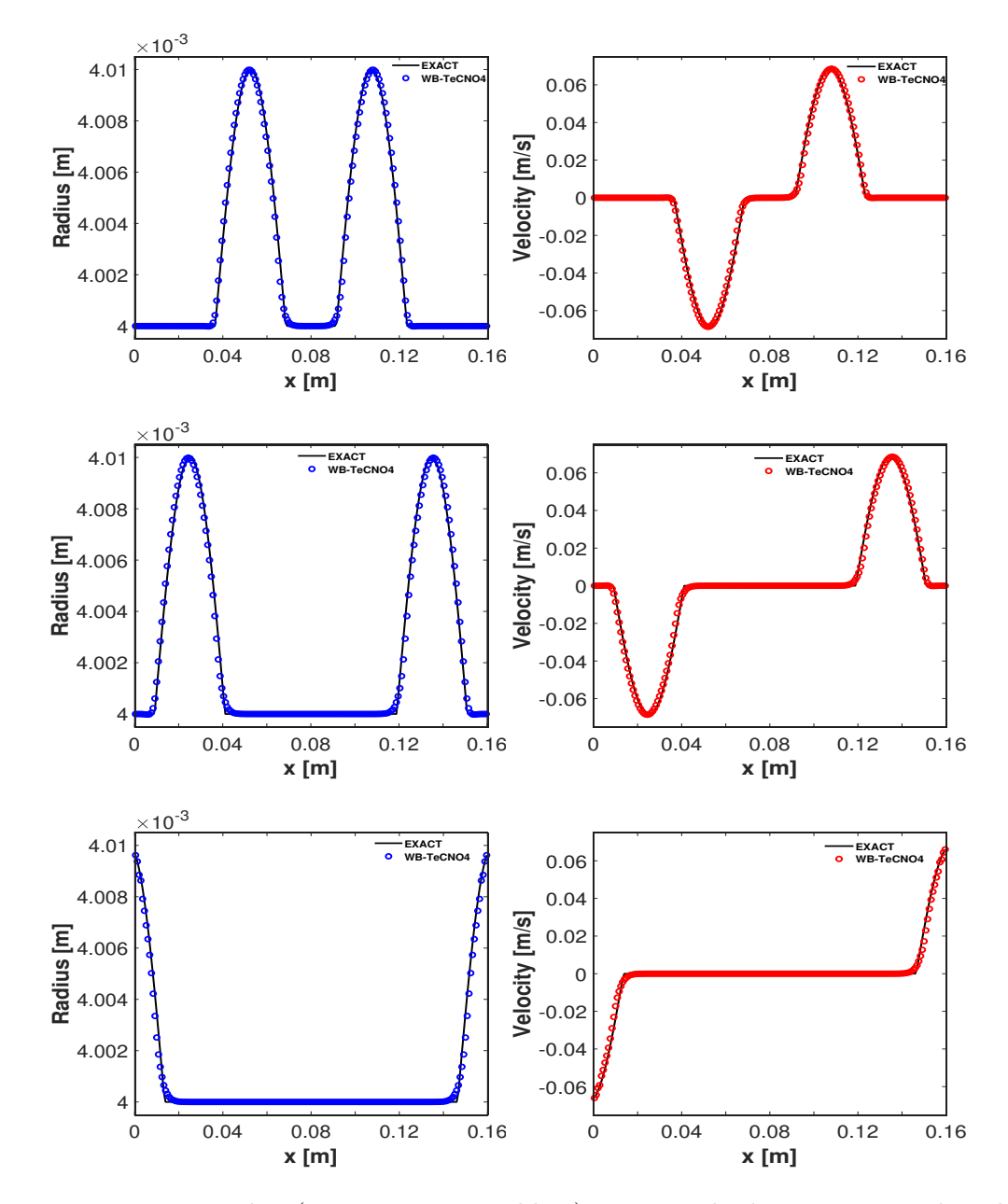


FIGURE 5. Example 4 (wave equation problem): numerical solutions on a mesh with 200 cells. Radius and velocity at simulated times t = 0.002 s (first row), t = 0.004 s (second row) and t = 0.006 s seconds (third row).

5.4. **Example 4: wave equation.** This example with constant cross-section at rest was proposed by Delestre and Lagrée [4]. It is chosen to show the capability of the proposed scheme to approximate the perturbed steady-state solutions. The cross section at rest is given by $A_0(x) = \pi R_0^2$ with $R_0 = 4 \times 10^{-3}$ m and the initial conditions are

$$A(x,0) = \begin{cases} \pi R_0^2 & \text{for } x \in [0, x_2] \cup [x_3, L], \\ \pi R_0^2 (1 + \varepsilon \sin(\pi(x - x_2)/x_1))^2 & \text{for } x \in [x_2, x_3] \end{cases} \quad \text{and} \quad U(x,0) = 0,$$

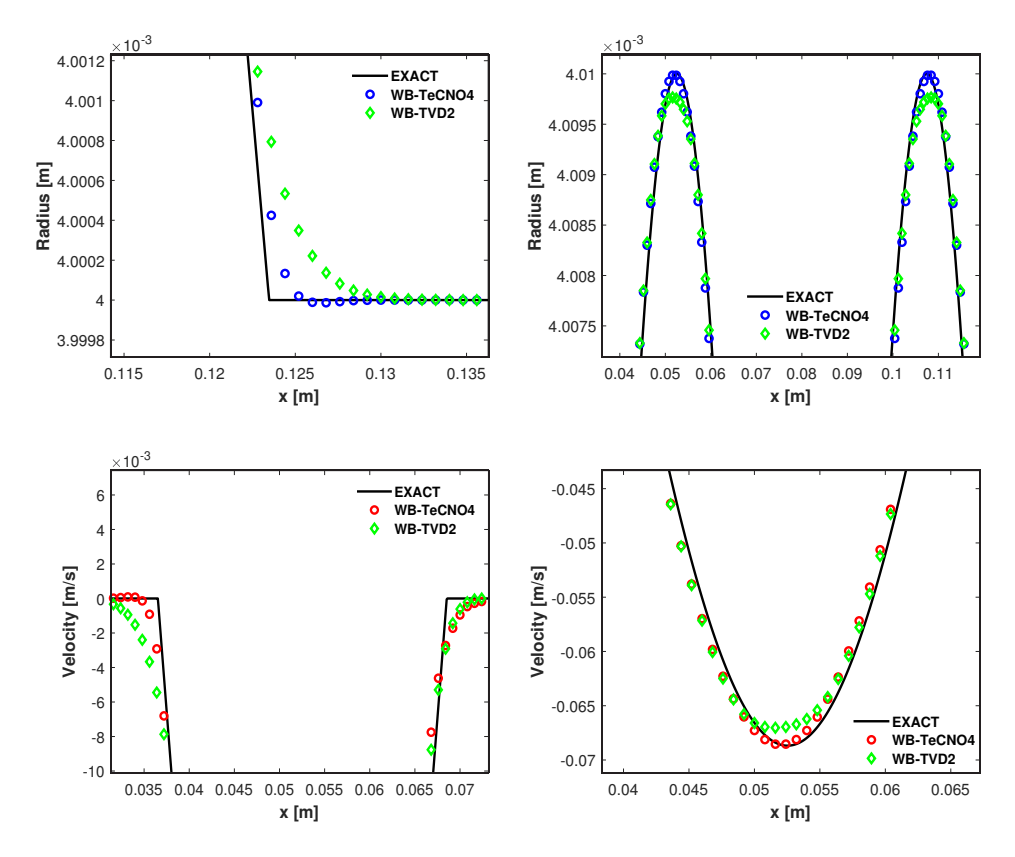


FIGURE 6. Example 4 (wave equation problem): enlarged views of numerical solutions at simulated time $t=0.002\,\mathrm{s}$ with M = 200 computed by WB-TeCNO4 and WB-TVD2.

with L = 0.16 m, $x_1 = 0.2L$, $x_2 = 0.4L$, $x_3 = 0.6L$ and $\varepsilon = 5 \times 10^{-3}$. The computational domain is [0, L] and $\beta = \pi^{-1} \times 10^8$ Pa/m. The exact solution (see [4]) can be expressed as

$$R(x,t) = R_0 + \frac{\varepsilon}{2} \left(\phi(x - c_0 t) + \phi(x + c_0 t) \right), \quad U(x,t) = -\varepsilon \frac{c_0}{R_0} \left(-\phi(x - c_0 t) + \phi(x + c_0 t) \right), \quad (5.2)$$

where $c_0 = c(A_0)$ and $\phi(x) = R_0 \sin(\pi(x - x_2)/x_1)\chi_{[x_2,x_3]}(x)$, where χ is the indicator function.

Figure 5 shows the numerical results at two different times, namely, $t = 0.002 \,\mathrm{s}$ and $t = 0.006 \,\mathrm{s}$ on a mesh with 200 cells. Comparison with the analytical exact solution given by (5.2) shows that small perturbations are well captured. We also include in Figures 6 and 7 enlarged views of numerical solutions of the wave equation by comparing the results produced by the WB-TeCNO4 scheme with those that are obtained from the entropy conservative flux (2.5) combined with a second-order total variation diminishing (TVD) reconstruction of the diffusion operator and the following second-order accurate discretization of the source term:

$$m{S}_j = rac{eta}{
ho} rac{1}{2\Delta x} \begin{pmatrix} 0 \\ A_{0,j-1}^{1/2} - A_{0,j-1}^{1/2} \end{pmatrix}.$$

This scheme is termed as WB-TVD2.

5.5. Example 5: propagation of a pulse to and from an expansion. This example models the reflection and the transmission of a small wave in an aneurysm when the cross section at rest

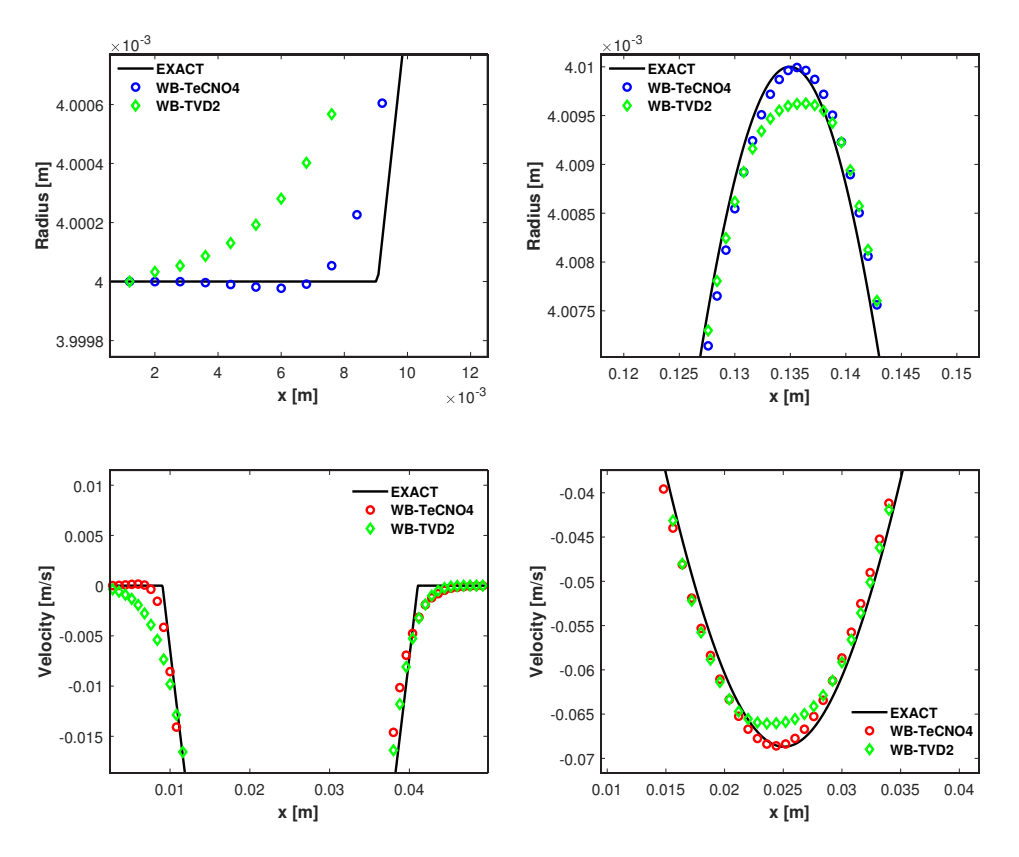


FIGURE 7. Example 4 (wave equation problem): enlarged views of numerical solutions at simulated time $t=0.004\,\mathrm{s}$ with M = 200 computed by WB-TeCNO4 and WB-TVD2

is not a constant [4]. The radius of the cross-section at rest is chosen as

$$R_0(x) = \begin{cases} \tilde{R} + \Delta R & \text{for } x \in [0, x_1], \\ \tilde{R} + \frac{\Delta R}{2} \left(1 + \cos \left(\frac{x - x_1}{x_2 - x_1} \pi \right) \right) & \text{for } x \in [x_1, x_2], \\ \tilde{R} & \text{otherwise} \end{cases}$$

with $\tilde{R} = 4 \times 10^{-3}$ m, $\Delta R = 1.0 \times 10^{-3}$ m, L = 0.16 m, $x_1 = 19L/40$, and $x_2 = L/2$. Initially, we describe a pulse propagating toward an expansion. The initial conditions are a fluid at rest U(x,0) = 0 and $A(x,0) = \pi [R(x,0)]^2$ with the perturbation of radius

$$R(x,0) = \begin{cases} R_0(x) (1 + \varepsilon \sin(5\pi(x - 0.65L)/L)) & \text{for } x \in [0.65L, 0.85L], \\ R_0(x) & \text{otherwise.} \end{cases}$$

Here, $\varepsilon = 5 \times 10^{-3}$ (see first row of Figure 8). Now, we simulate a pulse propagation from an expansion. In this case, the perturbation is initiated in the region of the vessel with larger area. The perturbed radius now becomes

$$R(x,0) = \begin{cases} R_0(x) (1 + \varepsilon \sin(5\pi(x - 0.15L)/L)) & \text{for } x \in [0.15L, 0.35L], \\ R_0(x) & \text{otherwise} \end{cases}$$

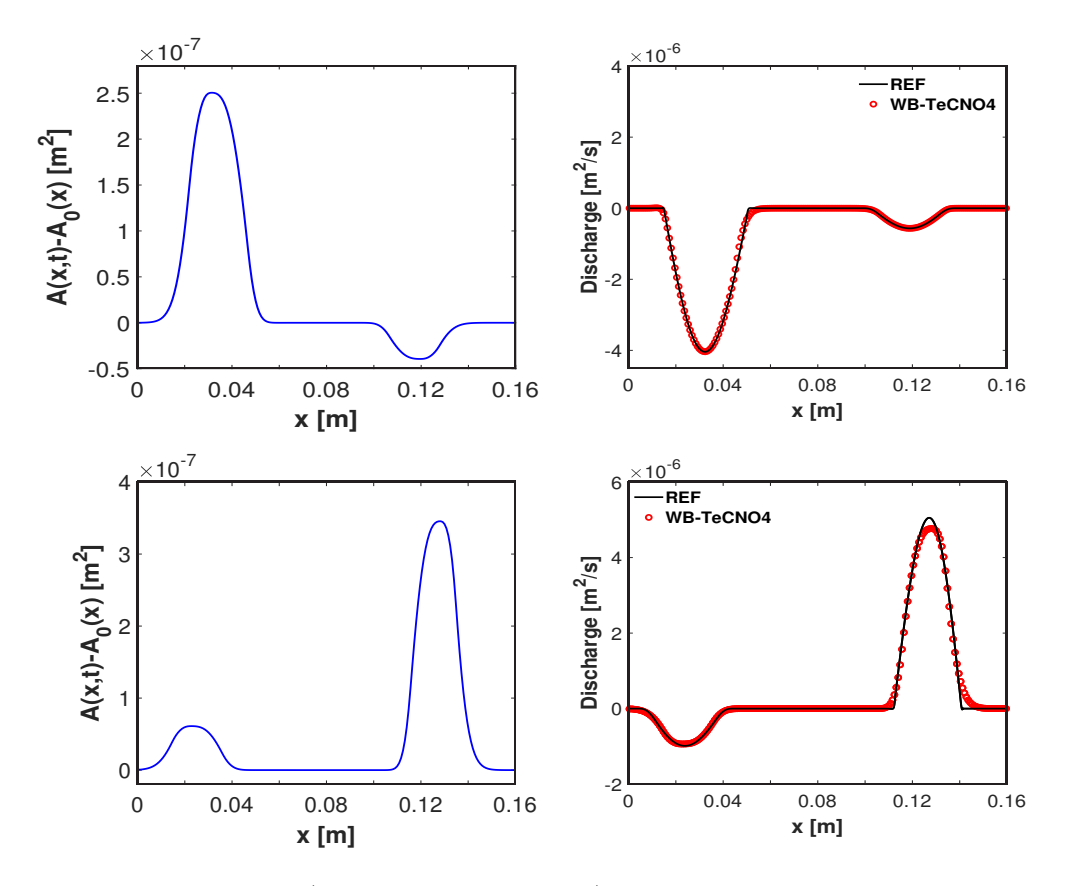


FIGURE 8. Example 5 (propagation of a pulse): numerical solutions of the propagation of a pulse (first row) toward an expansion and (second row) from an expansion, in both cases on a mesh with 200 cells, showing (left) the errors $A-A_0$ and (right) the discharge at simulated time t=0.006 s. The plots of discharge display the numerical solution values along with a reference solution (solid black line) corresponding to a reference solution with 4000 cells.

with the same value of ε . See the second row of Figure 8 for the numerical result.

6. Conclusions

In this paper, we have designed a very simple and computationally inexpensive well-balanced and entropy conservative finite volume scheme for a one-dimensional blood flow model which can preserve the man-at-eternal-rest steady state. Following [15, 16], numerical diffusion in terms of entropy variables was added to the entropy conservative scheme to obtain an entropy stable scheme. Some relevant numerical tests demonstrate that the proposed scheme preserves the steady state and gives good resolution for discontinuous solutions.

We comment here that satisfaction of the well-balanced property arises in a natural way from the design of the entropy conservative flux (2.6) in combination with the discretization of the source term (3.1). This approach provides an alternative to that of hydrostatic reconstruction (see, for example, [30]) that requires the computation of specific flux correction terms to achieve the well-balanced property. Furthermore, the diffusive correction introduced in Section 4 is zero whenever (3.4b) is in effect so the well-balanced property is not affected by the diffusive correction. In fact,

satisfaction of the well-balanced property of the present scheme should be related to the result by Wang et al. [13] who demonstrated that property (for the (A,Q) model) for all linear schemes, i.e., schemes that are based on approximating all spatial derivatives by a linear finite difference operator. These authors then argue that the WENO property of their approach, in principle, creates a nonlinear scheme due to the presence of nonlinear smoothness indicators and corresponding weights, and deal with this limitation by modifying the WENO scheme by a particular discretization of the source term. We emphasize that within our approach, the construction of entropy conservative fluxes produces a linear scheme, but the construction of diffusive corrections by ENO reconstruction introduces nonlinearity.

ACKNOWLEDGEMENTS

RB is acknowledges support by Fondecyt project 1210610; ANID/PIA/Concurso Apoyo a Centros Científicos y Tecnológicos de Excelencia con Financiamiento Basal AFB170001; and CRHIAM, project ANID/FONDAP/15130015.

References

- [1] S.J. Sherwin, V. Franke, J. Peiró, K. Parker, One-dimensional modelling of a vascular network in space-time variables, J. Eng. Math. vol. 47 (2003) pp. 217–250.
- [2] D. Xiu, S.J. Sherwin, Parametric uncertainty analysis of pulse wave propagation in a model of a human arterial network, Annals of Physics vol. 226 (2007) pp. 1385–1407.
- [3] L. Formaggia, F. Nobile, A. Quarteroni, A. Veneziani, Multiscale modelling of the circulatory system: a preliminar analysis, Comput. Visual. Sci. vol. 2 (1999) pp. 75–83.
- [4] O. Delestre, P.Y. Lagrée, A well-balanced finite volume scheme for blood flow simulation, Int. J. Numer. Methods Fluids vol. 72 (2013) pp. 177–205.
- [5] L. Formaggia, J.F. Gerbeau, F. Nobile, A. Quarteroni, On the coupling of 3D and 1D Navier-Stokes equations for flow problems in compliant vessels, Comput. Methods Appl. Mech. Engrg. vol. 191 (2001) pp. 561–582.
- [6] A.R. Ghigo, O. Delestre, J.M. Fullana, P.Y. Lagrée, Low-Shapiro hydrostatic reconstruction technique for blood flow simulation in large arteries with varying geometrical and mechanical properties, J. Comput. Phys. vol. 331 (2017) pp. 108–136.
- [7] E. Tadmor, The numerical viscosity of entropy stable schemes for systems of conservation laws. I, Math. Comp. vol. 49 (1987) pp. 91–103.
- [8] G. Langewouters, K. Wesseling, W. Goedhard, The elastic properties of 45 human thoracic and 20 abdominal aortas in vitro and the parameters of a new model, J. Biomech. vol. 17 (1984) pp. 425–435.
- [9] C. Sheng, S. Sarwal, K. Watts, A. Marble, Computational simulation of blood flow in human systemic circulation incorporating an external forced field, Med. Biol. Eng. Comput. vol. 33 (1995) pp. 8–17.
- [10] J.P. Mynard, P. Nithiarasu, A 1D arterial blood flow model incorporating ventricular pressure, aortic valve and regional coronary flow using the locally conservative Galerkin (LCG) method, Commun. Numer. Methods Engrg. vol. 24 (2008) pp. 367-417.
- [11] S. Acosta, C. Puelz, B. Rivière, D.J. Penny, C.G. Rusin, Numerical method of characteristics for one-dimensional blood flow, J. Comput. Phys. vol. 294 (2015) pp. 96–109.
- [12] E. Boileau, P. Nithiarasu, P.J. Blanco, L.O. Müller, F.E. Fossan, L.R. Hellevik, W.P. Donders, W. Huberts, M. Willemet, and J. Alastruey, A benchmark study of numerical schemes for one-dimensional arterial blood flow modelling, Int. J. Numer. Meth. Biomed. Engng. vol. 31 (2015) pp. 1–33.
- [13] Z. Wang, G. Li, O. Delestre, Well-balanced finite difference weighted essentially non-oscillatory schemes for the blood flow model, Int. J. Numer. Methods Fluids vol. 82 (2016) pp. 607–622.
- [14] C. Puelz, S. Canic, B. Rivière, C.G. Rusin, Comparison of reduced models for blood flow using Runge-Kutta discontinuous Galerkin methods, Appl. Numer. Math. vol. 115 (2017) pp. 114–141.
- [15] E. Tadmor, Entropy stability theory for difference approximations of nonlinear conservation laws and related time-dependent problems, Acta Numerica vol. 12 (2003) pp. 451–512.
- [16] U.S. Fjordholm, S. Mishra, E. Tadmor, Arbitrarily high-order accurate entropy stable essentially nonoscillatory schemes for systems of conservation laws, SIAM J. Numer. Anal. vol. 50 (2012) pp. 544–573.

- [17] P.G. Lefloch, J.M. Mercier, C. Rohde, Fully discrete entropy conservative schemes of arbitrary order, SIAM J. Numer. Anal. vol. 40 (2002) pp. 1968–1992.
- [18] M.J. Castro, U.S. Fjordholm, S. Mishra, C. Parés, Entropy conservative and entropy stable schemes for nonconservative hyperbolic systems, SIAM J. Numer. Anal. vol. 51 (2013) pp. 1371–1391.
- [19] U.S. Fjordholm, S. Mishra, Accurate numerical discretizations of non-conservative hyperbolic systems, ESAIM: Math. Model. Numer. Anal. vol. 46 (2012) pp. 187–206.
- [20] A. Hiltebrand, S. Mishra, Entropy stable shock capturing spacetime discontinuous Galerkin schemes for systems of conservation laws, Numer. Math. vol. 126 (2014) pp. 103–151.
- [21] U.S. Fjordholm, S. Mishra, E. Tadmor, Well-balanced and energy stable schemes for the shallow water equations with discontinuous topography, J. Comput. Phys. vol. 230 (2011) pp. 5587–5609.
- [22] U.S. Fjordholm, S. Mishra, E. Tadmor, Energy preserving and energy stable schemes for the shallow water equations. In: Foundations of Computational Mathemathics, F. Cucker, A. Pinkus, and M. Todd (Eds.), Proceedings of FoCM held in Hong Kong, London Math. Society Lecture Notes Ser. vol. 363, Cambridge University Press, 2008, pp. 93–139.
- [23] E. Tadmor, Entropy stable schemes, Chapter 18 in R. Abgrall and C.-W. Shu (eds.), Handbook of Numerical Methods for Hyperbolic Problems: Basic and Fundamental Issues, vol. 17 of Handbook of Numerical Analysis, North-Holland, Amsterdam, 2016, pp. 467–493.
- [24] J.S. Hesthaven, Numerical Methods for Conservation Laws, SIAM, Philadelphia, 2018.
- [25] S. Benzoni-Gavage, R.M. Colombo, An n-populations model for traffic flow, European J. Appl. Math. vol. 14 (2003) pp. 587–612.
- [26] R. Bürger, K.H. Karlsen, J.D. Towers, On some difference schemes and entropy conditions for a class of multispecies kinematic flow models with discontinuous flux, Netw. Heterog. Media vol. 5 (2010) pp. 461–485.
- [27] R. Bürger, H. Torres, C.A. Vega, An entropy stable scheme for the multiclass Lighthill-Whitham-Richards traffic model, Adv. Appl. Math. Mech. vol. 11 (2019) pp. 1022–1047.
- [28] S. Jerez, C. Parés, Entropy stable schemes for degenerate convection-diffusion equations, SIAM J. Numer. Anal. vol. 55 (2017) pp. 240–264.
- [29] R. Bürger, P.E. Méndez, C. Parés, On entropy stable schemes for degenerate parabolic multispecies kinematic flow models, Numer. Methods Partial Differential Eq. vol. 35 (2019) pp. 1847–1872.
- [30] G. Li, O. Delestre, Y. Yuan, Well-balanced discontinuous Galerkin method and finite volume WENO scheme based on hydrostatic reconstruction for blood flow model in arteries, Int. J. Numer. Methods Fluids vol. 86 (2020) pp. 491–508.
- [31] T.J. Barth, Numerical methods for gas-dynamics systems on unstructured meshes. In: An Introduction to Recent Developments in Theory and Numerics of Conservation Laws, D. Kröner, M. Ohlberger, and C. Rohde (Eds.): Lecture Notes in Comput. Sci. Engrg., Springer, Berlin, vol. 5 (1999) pp. 195–285.
- [32] S. Gottlieb, C.-W. Shu, E. Tadmor, Strong stability-preserving high-order time discretization methods, SIAM Rev. vol. 43 (2001) pp. 89–112.
- [33] J. Britton, Y. Xing, Well-balanced discontinuous Galerkin methods for the one-dimensional blood flow through arteries model with man-at-eternal-rest and living-man equilibria, Computers & Fluids vol. 203 (2020) pp. 1–32.